Understanding Nucleic Acid Structural Changes by Comparing Wide-Angle X-ray Scattering (WAXS) Experiments to Molecular Dynamics Simulations

Suzette A. Pabit,[1] Andrea M. Katz,[1] Igor S. Tolokh,[2] Aleksander Drozdetski,[3] Nathan Baker,[4] Alexey V. Onufriev,[2, 3] and Lois Pollack[1]

[1] *School of Applied and Engineering Physics, Cornell University, Ithaca, NY 14853, USA*

[2] *Department of Computer Science, Virginia Tech, Blacksburg, VA 24061, USA*

[3] *Department of Physics, Virginia Tech, Blacksburg, VA 24061, USA*

[4] *Pacific Northwest National Laboratory, Richland, WA 99352, USA*

(Dated: 29 December 2015)

Wide-angle x-ray scattering (WAXS) is emerging as a powerful tool for increasing the resolution of solution structure measurements of biomolecules. Compared to its better known complement, small angle x-ray scattering (SAXS), WAXS targets higher scattering angles and can enhance structural studies of molecules by accessing finer details of solution structures. Although the extension from SAXS to WAXS is easy to implement experimentally, the computational tools required to fully harness the power of WAXS are still under development. Currently, WAXS is employed to study structural changes and ligand binding in proteins; however the methods are not as fully developed for nucleic acids. Here, we show how WAXS can qualitatively characterize nucleic acid structures as well as the small but significant structural changes driven by the addition of multivalent ions. We show the potential of WAXS to test all-atom molecular dynamics (MD) simulations and to provide insight in understanding how the trivalent ion cobalt(III) hexammine (CoHex) affects the structure of RNA and DNA helices. We find that MD simulations capture the RNA structural change that occurs due to addition of CoHex.

The accessibility of synchrotron radiation sources for Small Angle X-ray Scattering (SAXS) experiments has enabled new methods for measuring low resolution structures of biological macromolecules[1,2]. The spatial resolution d of a SAXS measurement is largely determined by the highest q value of the measurement, given by $d = 2\pi/q$, where q is the momentum transfer, $q = (4\pi/\lambda) \cdot \sin(2\theta/2)$, λ is the x-ray wavelength and 2θ is the scattering angle. Extension from small-angle to wide-angle x-ray scattering (WAXS) is appealing because scattering at wider angles yields higher resolution structural features[3,4]. For example, even a modest maximum q at around 1.0 Å^{-1} corresponds to features that are in the $5 - 10$ Å spatial range. Implementation of WAXS is simple and often requires a trivial modification to a SAXS beamline: the detector is moved closer to the sample to capture x-rays scattered to higher angles. It is even possible to simultaneously acquire SAXS and WAXS data by placing a detection window near the sample[5]. WAXS provides information about length scales of critical structural importance, and is particularly relevant for studies of nucleic acid structures. For example, in DNA, peaks in the WAXS regime of $0.4 < q < 1.0$ Å^{-1} arise from interstrand pair distance correlations from major and minor groove spacing and helix radius[6].

Despite the relative ease of acquiring WAXS data, the challenge in its application arises from the interpretation of the measured scattering profiles. On these shorter length scales, for example, the contribution of the solvent, including the hard-to-model hydration shell around biomolecules, becomes significant[7]. A number of experimental and computational tools for the analysis of WAXS structures of biomolecules are available but all rely on the availability of high resolution atomic coordinates for comparison[4,8,9]. Since atomic coordinates are not readily available for many biomolecules, this limits the applicability of WAXS analysis software. Moreover, most of these analysis tools are geared towards studies of protein structural fluctuations and protein ligand binding[4,10,11], where the hydration layer is reasonably well described. In contrast, because of the highly charged nature of nucleic acids, accurate models of the dense solvent layer adjacent to the molecule are still under development. A method to calculate nucleic acid SAXS and WAXS profiles that includes not only the hydration shell, but also charge compensating counterions has recently been introduced[12] but still requires input of matching atomic coordinates of nucleic acids structures.

The goal of this paper is to extend the use of WAXS to studies of nucleic acids. We discuss two cases where interpretation of WAXS experimental data is possible. First, when key structural features are present in the nucleic acid scattering profiles, we can compare the location of the peaks and valleys to those calculated from existing structural models of nucleic acids based on canonical helices and Molecular Dynamics (MD) simulation results. In this way, WAXS data can help guide the development and refinement of MD simulations. When data and models agree, MD results can help visualize WAXS-resolved structural features. The second way to interpret nucleic acid WAXS data is to look at changes in the WAXS profiles induced by the addition of ligands or multivalent ions. Intensity difference curves have been used in the study of WAXS structures in proteins, particularly for comparing different time points in time-resolved experiments[13,14]. Here, we show that a comparison of in-
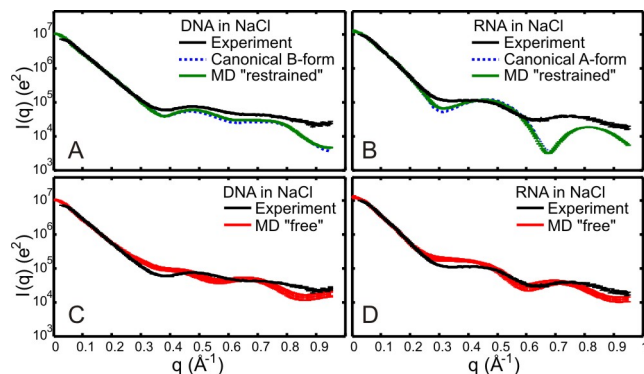
FIG. 1. Comparison of wide-angle scattering data from (A) DNA and (B) RNA in 100 mM NaCl to canonical helices built using Nucleic Acid Builder (NAB) and structural ensembles generated by "restrained" MD simulations. The small differences between NAB and "restrained" MD reflects the small deviation from the restraining harmonic potential. A similar comparison is made between (C) DNA and (D) RNA data and "free" MD structures after the restraining force is removed.

tensity difference curves (MD to experiment) is a useful way to interpret changes in the nucleic acid structure on the nanometer length scale.

Double-stranded 25 base-pair (bp) DNA and RNA constructs were annealed from single-stranded nucleic acids purchased from IDT (Coralville, IA). We used the same mixed sequence described in our previous publications, GCA TCT GGG CTA TAA AAG GGC GTC G (U replacing T for the RNA strands)[15,16]. Cobalt(III) Hexammine chloride, $Co(NH_3)_6Cl_3$ (CoHex), sodium chloride, NaCl, and the buffers used were purchased from Sigma-Aldrich (St. Louis, MO). The duplexes were extensively dialyzed using Amicon Ultra Concentrators (Millipore, Billerica, MA) in pH 7.0 Na-MOPS buffer containing either 100 mM NaCl only or 100 mM NaCl and 0.8 mM $Co(NH_3)_6Cl_3$. The monovalent salt concentrations were chosen to prevent trivalent CoHex induced precipitation and focus the study on CoHex-nucleic acid interactions in the pre-condensed solution phase. The WAXS experiments were carried out at the G1 station at the Cornell High Energy Synchrotron Source (CHESS). Using a scattering flight path with a 0.455 m sample to detector distance, we reached a $q_{max} = 0.95$ Å^{-1}, which is sensitive to correlation lengths of $d_{min} = 2\pi/q_{max} = 6.6$ Å. This allows us to target the WAXS region of $0.4 < q < 0.95$ Å^{-1} which is corresponds to the length scales of the helix radius and the minor and major groove spacing[6]. We purposely avoid $q > 1.0$ Å^{-1} where contributions from solvent scattering become more intense[4]. The x-ray energy used was 10.60 keV and scattered x-rays were imaged using a low-noise photon counting area detector (Pilatus 100K, Dectris, Baden, Switzerland). Duplex concentrations were about 450 μM. The samples, with volumes of about 30 μL, were kept in a 2-mm quartz capillary (Hampton Research, Aliso Viejo, CA) and radiation damage was avoided by oscillating the sample during

the data collection. Signals from the buffer background were subtracted from the data and absolute calibration was performed using water as a calibrant as described previously[12,17]. A more detailed description of the experimental measurements are provided in Ref.[12].

MD simulations of RNA and DNA constructs in explicit water and monovalent ions (NaCl) were carried out in the presence and absence of CoHex ions using AMBER 12 and ff99bsc0 force fields[18–20]. The starting structures for the MD simulations were generated from canonical helices (A-form for RNA and B-form for DNA) built using Nucleic Acid Builder (NAB)[21]. Simulation details are similar to those described in Ref.[16]. In the first 140 ns of simulation, a restraining harmonic potential with a force constant of 50 kcal/mol/Å^2 was applied to the canonical forms of the RNA and DNA molecules. The restraining force was removed and the simulations were allowed to proceed for another 100-200 ns. To compare the MD results with the WAXS data, we extracted 100-500 snapshots from each trajectory in PDB format and generated WAXS profiles using the program CRYSOL[22]. CRYSOL is a commonly-used program for calculating the solution scattering profiles of macromolecules with known atomic coordinates. Though other WAXS solvers are available and a simple test of the program WAXSiS[9] yielded similar profiles, we chose CRYSOL for speed of the calculations and ease of handling hundreds of PDB snapshots. The CRYSOL input settings were configured so that the output scattering profiles are fitted to the experimental data. All other parameters were set to the CRYSOL default values (e.g. solvent density set to pure water). We report all CRYSOL results in absolute intensity units (e^2). To focus on the nucleic acid structural features, the ions were not included in the CRYSOL calculations unless otherwise indicated in the text. Profiles generated from hundreds of PDB snapshots were pooled together into two groups, MD profiles with the restraining force in place ("restrained" profiles) and MD profiles after the restraining force was released ("free" profiles). The pools were averaged and these averages were compared to the data.

Figure 1 compares background subtracted experimental WAXS profiles of nucleic acids in NaCl to canonical helices and MD simulation profiles. We show intensity, I vs. q curves in logarithmic scale to enhance structural features in the WAXS regime, the higher-q region of the dataset ($q > 0.4$ Å^{-1}). Displaying the data in this form allows us to easily assess whether the general features and peaks of the experimental profiles agree or disagree with the simulations and the canonical helices built using NAB. In Figure 1A, we compare our experimental profiles of DNA in NaCl to a canonical B-form helix and MD simulations in NaCl and explicit water with the restraining force in place ("restrained" profiles). Since the "restrained" MD models are derived from NAB, the calculated profiles are very similar with very small deviations due to the restraining harmonic potential. Note the relative agreement between the experiment and the
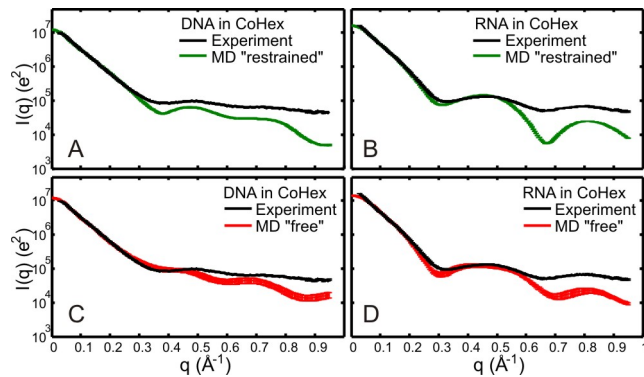
FIG. 2. Comparison of wide-angle scattering data from nucleic acids in 0.8 mM CoHex and 100 mM NaCl solution to "restrained" and "free" MD simulations. (A) and (C) are for DNA and (B) and (D) are for RNA. The number of CoHex and NaCl in the simulation box complements the experiment.

calculated "restrained" MD and NAB profiles, exhibiting the characteristic features that were seen in previous measurements[6] on B-form DNA with a peak measured at $q = 0.48$ Å^{-1} and a shallow peak detected at $q = 0.72$ Å^{-1}. Although agreement is qualitative, the peak positions are in the right place. Thus, scattering profiles for DNA in NaCl compare favorably with predictions of "restrained" MD simulations, suggesting that the B-form structure is relatively robust. In contrast, the scattering profile of RNA in NaCl shown in Figure 1B looks substantially different from the "restrained" MD profiles. As expected, the MD simulations results using "restrained" RNA recapitulate the features exhibited in the NAB canonical A-form structure because of the restraining potential. However, both curves disagree with the experimental data. The first peak in the experimental WAXS profiles for RNA is too shallow (more like a shoulder than a peak) and shifted to the left compared to the "restrained" MD profile, the second peak is also shifted to the left.

In Figures 1C and 1D, we compare the experimental data with the MD simulation results after the restraining force has been released ("free" profiles). Interestingly, the WAXS profiles computed for "free" DNA, Figure 1C, no longer capture the agreement with experiment as seen in the "restrained" models. The peak positions are completely different and the simulation curves appear out-of-phase with the data. On the other hand, the features of the RNA WAXS data in NaCl are better captured by the MD simulations after the restraining force has been released. In Figure 1D, we note that the shoulder in the "free" MD near $q = 0.4$ Å^{-1} also appears in the experimental curves. However, the second peak position is not exactly in the same place. Nonetheless, at $q = 0.71$ Å^{-1}, it is closer to the experimental peak at $q = 0.74$ Å^{-1} than the peak value of $q = 0.82$ Å^{-1} for the "restrained" MD. This result suggests that in an NaCl solution, duplex RNA does not have a rigid canonical A-form structure.

The limitations of MD force-fields for DNA have been

thoroughly discussed in a paper by Tiede and coworkers where they benchmarked the WAXS profiles to MD solutions and found a need to develop experimentally validated, supramolecular force fields[6]. Our findings reiterate theirs, and further the field by reporting results with RNA. What is surprising here is the better agreement between the unrestrained MD and the experimental data in RNA. The disagreement between our DNA WAXS data and the structures from the "free" MD for DNA arise from deviations (drift towards A-like conformations) of key structural features in the MD-generated ensemble from the values expected for canonical B-form DNA. Force field modification is beyond the scope of this work, however, we illustrate the use of WAXS as an experimental test. While the WAXS curves are not exactly predicted (on an absolute scale) by the force field, they present qualitative features that accurately reflect structural features of these duplexes, hence provide a useful experimental metric.

In Figure 2, we examine structural changes in DNA and RNA induced by the addition of multivalent ions. Cobalt(III) Hexammine, $[Co(NH_3)_6]^{3+}$ or CoHex, is a trivalent ion that is widely used to facilitate and study DNA condensation[23,24]. This highly charged spherical ion has a dramatically different effect on short double helices made of DNA and RNA. The addition of a small amount of CoHex ions precipitates short DNA helices from solution, while RNA molecules of similar sequence remain soluble[15,16]. The efficiency of condensation appears to be primarily related to the mode of CoHex binding, which is mostly determined by the helix geometry, although other factors like nucleotide sequence do contribute. Simulations of B-form DNA suggest that CoHex ions decorate the outer surface of the structure, while MD simulations of A-like RNA suggest that the ions are drawn deep into the negatively charged major groove. A discussion of how ion placement influences precipitation can be found in our previous work, Ref.[16], where UV spectroscopy and circular dichroism (CD) were used to monitor precipitation and helical form, and the MD simulations of different duplexes were described. However, a limitation of this previous study[16] lies in our inability to directly compare MD simulations to experimental data. Although CD reports spectral changes in RNA, there is no straightforward way to correlate the changes in nucleic acid CD spectra with MD predictions. In fact, our attempts to use the CD modeling software Dichrocalc[25], which was written for proteins, yielded results that substantially differ from the CD data. Here, we explore the use of WAXS as an experimental way to check if changes in the structures of DNA and RNA duplexes due to CoHex are predicted by simulation.

Although the signal from the CoHex ions is too small to be detected experimentally in the WAXS profiles, CoHex-driven changes in local structure, suggested by the CD data, should be noticeable. Figure 2 shows WAXS profiles of the nucleic acids in a CoHex-NaCl solution and compares the profiles with simulations. Although we ob-

serve some lineshape broadening in the WAXS peaks of the DNA samples, the peak positions do not move after addition of CoHex. The same B-form DNA structure is still captured in Figure 2A with "restrained" MD. This behavior is expected from DNA molecules since Circular Dichroism (CD) measurements showed that CD changes in DNA with and without CoHex are minimal while a large spectral shift in the CD spectra for RNA was observed upon addition of CoHex[16]. In agreement with CD, distinct changes are observed in the RNA WAXS profiles upon addition of CoHex. In fact, in the presence of CoHex, the WAXS structures of RNA appear more like canonical A-form helix and have peaks in similar positions to the "restrained" MD (Figure 2B). Similar to DNA in NaCl, the "free" MD profiles for DNA in CoHex show disagreement in peak positions (Figure 2C). For RNA, peak positions in the "free" MD profiles qualitatively agree with the data.

To better compare changes in structural features in WAXS profiles due to addition of CoHex, we look at differences in the scattering intensity following the method used in Refs.[4,13,14,26]. In Figure 3, we show experimental intensity difference profiles, $\log(I_{NaCl}) - \log(I_{CoHex})$, and compare them to the difference profiles computed from the simulated curves. Since all the experimental data shown have absolute calibration and the MD profiles calculated using CRYSOL are made to fit the data, no scaling was applied prior to the subtraction. Looking at all panels in Figure 3, we immediately see that the key features in the intensity difference curves are best captured by MD results shown in Figure 3D where unrestrained or "free" MD difference profiles are compared to the experimental difference profiles for RNA. The difference peaks at $q = 0.3$ Å^{-1} and at $q = 0.7$ Å^{-1} in the RNA experimental curves also appear in the MD simulations albeit with different amplitudes. This result is quite interesting: it suggests that CoHex-induced changes the RNA structure are well-represented in the "free" MD simulations after the restraining force on RNA has been removed.

MD models of DNA are harder to describe because features in the difference profiles are not as distinct as they are for RNA. However, even with less pronounced features, we find that the DNA data are more consistent with MD results from "restrained" DNA, not "free" DNA. The "restrained" MD-derived difference curve is largely featureless (Figure 3A) while the 'free' MD-derived difference curve (Figure 3C) has peaks and valleys whose locations are inconsistent with the data. Figure 3B for "restrained" RNA also shows disagreement in the position of peaks and valleys. Thus, we find that comparison of intensity difference curves to models is not only a useful way to denote changes in the nucleic acid structure, but is also a robust method to identify good models and discard models that do not reflect experimental data. The agreement in Figure 3D between MD and experiment is still qualitative but the disagreement in Figure 3B and 3C is quite notable.
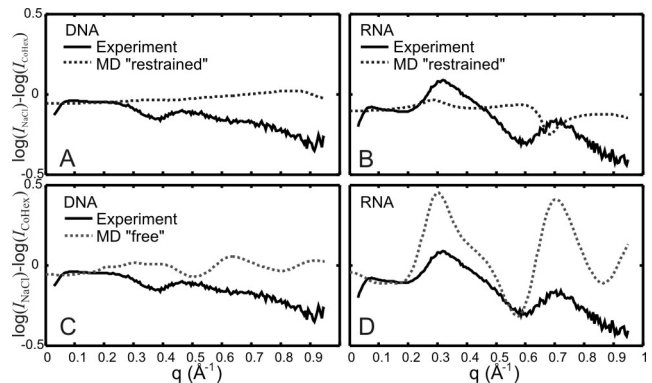
These results can now be used to gain physical insight

FIG. 3. Intensity difference profiles, $\log(I_{NaCl}) - \log(I_{CoHex})$, comparing nucleic acid experimental data to MD results when the molecules are "restrained" by a harmonic potential (A and B) and when molecules are "free" (C and D). The figure legends shown in panel (C) for DNA also apply to panel (D) for RNA. The best qualitative agreement with experiment happens when RNA is unrestrained in the MD simulations.

into the origin of the structural changes. The need to use unrestrained "free" MD simulations for RNA suggests that CoHex introduces structural changes to the A-form helix. In Figure 4, we show experimental WAXS profiles, I vs. q, in logarithmic scale, comparing RNA to "free" MD results and the canonical A-form helix from NAB. Without CoHex, Figure 4A shows RNA experimental profiles favoring the "free" MD profiles with the shoulder around $q = 0.45$ Å^{-1}. However, the shallow peak seen in the data at $q = 0.74$ Å^{-1} is shifted to the left in the MD simulations (peak at $q = 0.71$ Å^{-1}). In the presence of CoHex (Figure 4B), both RNA experimental curves and the results from the "free" MD appear to have features more similar to the canonical A-form profile. When the ions are turned off in CRYSOL (our default setting), the second peak around $q = 0.81$ Å^{-1} becomes more pronounced in the "free" MD profile with CoHex, which implies that CoHex changes the actual structure of the RNA, not just the counterion cloud or the hydration layer. The smearing of the $q = 0.81$ Å^{-1} peak when ions are turned on suggests diffuse positioning of the CoHex ions in the vicinity of $d = 2\pi/q = 7.8$ Å, consistent with our picture of CoHex ions deep in the A-form major groove[16]. Figure 4 insets show representative snapshots of the RNA structure from the unrestrained MD simulation with and without CoHex. From the pool of MD-derived PDB snapshots, we measured the average distance between the 3'-end phosphates of the base-paired strands. The end-to-end phosphate distance for the RNA in NaCl was 75 ± 3 Å vs. 66 ± 2 Å for the RNA in CoHex/NaCl suggesting a shortening of the structure in the presence of CoHex.

In summary, we compared MD-derived structures to experimental WAXS data and showed the power of WAXS in investigating nucleic acid structural features and structural changes. Although our analysis of WAXS data is currently limited by the need to compare to acces-
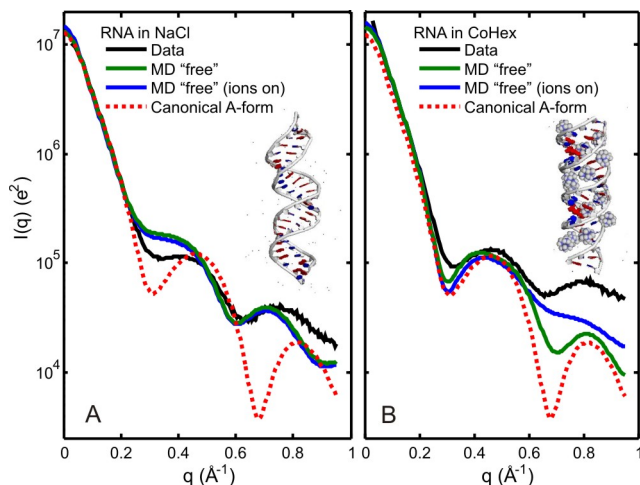
FIG. 4. WAXS profiles comparing RNA data to "free" MD and the canonical A-form helix from NAB in (A) NaCl only and (B) NaCl/CoHex solution. Insets show representative structures of RNA from MD snapshots. Double-stranded RNA with CoHex appears to have a shorter end-to-end distance and a WAXS profile that has features more similar to the canonical A-form helix.

sible PDB structures, comparison of intensity difference profiles from experimental data and those generated from MD-derived models provides a test of MD simulation predictions. Changes in RNA WAXS data with and without CoHex ions were well represented by changes in profiles computed from structures generated in unrestrained MD simulations. Changes in experimental DNA WAXS profiles are smaller and are consistent with the need to restrain DNA structures during long (hundreds of nanoseconds) MD simulations. Thus, we experimentally validated our use of MD models in a previous publication[16]: "restrained" for DNA and "free" for RNA, to explain condensation propensity and discern CoHex binding modes. This practical and heretofore unknown result, validating RNA MD structures with data, allowed us to demonstrate that CoHex affects RNA helices by shortening end-to-end distance and forcing the molecule to adapt a more A-like conformation. The future application of computational methods that allow MD simulations to be guided by SAXS and WAXS data, a process that is currently being developed for proteins[27], holds great potential for studies of nucleic acids.

ACKNOWLEDGMENTS

[1] J. Pérez and Y. Nishino, "Advances in X-ray scattering: From solution SAXS to achievements with coherent beams," Current Opinion in Structural Biology **22**, 670–678 (2012).

[2] S. Skou, R. E. Gillilan, and N. Ando, "Synchrotron-based small-angle X-ray scattering of proteins in solution." Nature protocols **9**, 1727–39 (2014).

[3] M. A. Graewert and D. I. Svergun, "Impact and progress in small and wide angle X-ray scattering (SAXS and WAXS)," Current Opinion in Structural Biology **23**, 748–754 (2013).

[4] L. Makowski, "Characterization of proteins with wide-angle X-ray solution scattering (WAXS)," Journal of Structural and Functional Genomics **11**, 9–19 (2010).

[5] M. Allaire and L. Yang, "Biomolecular solution X-ray scattering at the national synchrotron light source," Journal of Synchrotron Radiation **18**, 41–44 (2011).

[6] X. Zuo, G. Cui, K. M. Merz, L. Zhang, F. D. Lewis, and D. M. Tiede, "X-ray diffraction fingerprinting of DNA structure in solution for quantitative evaluation of molecular dynamics simulation," PNAS **103**, 3534–9 (2006).

[7] S. Park, J. P. Bardhan, B. Roux, and L. Makowski, "Simulated x-ray scattering of protein solutions using explicit-solvent models," Journal of Chemical Physics **130**, 134114 (2009).

[8] J. Bardhan, S. Park, and L. Makowski, "SoftWAXS: A computational tool for modeling wide-angle X-ray solution scattering from biomolecules," Journal of Applied Crystallography **42**, 932–943 (2009).

[9] C. J. Knight and J. S. Hub, "WAXSiS: a web server for the calculation of SAXS/WAXS curves based on explicit-solvent molecular dynamics," Nucleic Acids Research **43**, W225–W230 (2015).

[10] J. J. Virtanen, L. Makowski, T. R. Sosnick, and K. F. Freed, "Modeling the hydration layer around proteins: Applications to small- and wide-angle X-ray scattering," Biophysical Journal **101**, 2061–2069 (2011).

[11] D. D. L. Minh and L. Makowski, "Wide-angle X-ray solution scattering for protein-ligand binding: Multivariate curve resolution with bayesian confidence intervals," Biophysical Journal **104**, 873–883 (2013).

[12] H. T. Nguyen, S. A. Pabit, S. P. Meisburger, L. Pollack, and D. A. Case, "Accurate small and wide angle x-ray scattering profiles from atomic models of proteins and nucleic acids," The Journal of Chemical Physics **141**, 22D508 (2014).

[13] M. Cammarata, M. Levantino, F. Schotte, P. a. Anfinrud, F. Ewald, J. Choi, A. Cupane, M. Wulff, and H. Ihee, "Tracking the structural dynamics of proteins in solution using time-resolved wide-angle X-ray scattering." Nature methods **5**, 881–886 (2008).

[14] D. Arnlund, L. C. Johansson, C. Wickstrand, A. Barty, and G. J. Williams, "Visualizing a protein quake with time-resolved X-ray scattering at a free-electron laser," Nature Methods **11** (2014).

[15] L. Li, S. A. Pabit, S. P. Meisburger, and L. Pollack, "Double-stranded RNA resists condensation," Physical Review Letters **106**, 108101 (2011).

[16] I. S. Tolokh, S. A. Pabit, A. M. Katz, Y. Chen, A. Drozdetski, N. Baker, L. Pollack, and A. V. Onufriev, "Why double-stranded RNA resists condensation." Nucleic acids research **42**, 10823–10831 (2014).

[17] D. Orthaber, A. Bergmann, and O. Glatter, "SAXS experiments on absolute scale with Kratky systems using water as a secondary standard," Journal of Applied Crystallography **33**, 218–225 (2000).

[18] D. A. Case, T. E. Cheatham, T. Darden, H. Gohlke, R. Luo, K. M. Merz, A. Onufriev, C. Simmerling, B. Wang, and R. J.

Woods, "The Amber biomolecular simulation programs." Journal of computational chemistry **26**, 1668–88 (2005).

[19] T. E. Cheatham, P. Cieplak, and P. A. Kollman, "A modified version of the Cornell et al. force field with improved sugar pucker phases and helical repeat." Journal of biomolecular structure & dynamics **16**, 845–862 (1999).

[20] A. Pérez, I. Marchán, D. Svozil, J. Sponer, T. E. Cheatham, C. A. Laughton, and M. Orozco, "Refinement of the AMBER force field for nucleic acids: improving the description of alpha/gamma conformers." Biophysical journal **92**, 3817–29 (2007).

[21] T. Macke and D. A. Case, "Molecular Unusual Nucleic Acid Structures," in *Molecular Modeling of Nucleic Acids*, edited by N. B. Leontes and J. SantaLucia Jr. (American Chemical Society, Washington DC, 1998) pp. 379–393.

[22] D. Svergun, C. Barberato, and M. H. Koch, "CRYSOL - A program to evaluate X-ray solution scattering of biological macromolecules from atomic coordinates," Journal of Applied Crystallography **28**, 768–773 (1995).

[23] J. Widom and R. L. Baldwin, "Cation-induced toroidal condensation of DNA studies with Co3+(NH3)6." Journal of molecular biology **144**, 431–453 (1980).

[24] J. Pelta, F. Livolant, and J. L. Sikorav, "DNA aggregation induced by polyamines and cobalthexamine," Journal of Biological Chemistry **271**, 5656–5662 (1996).

[25] B. M. Bulheller and J. D. Hirst, "DichroCalc - Circular and linear dichroism online," Bioinformatics **25**, 539–540 (2009).

[26] R. F. Fischetti, D. J. Rodi, D. B. Gore, and L. Makowski, "Wide-angle X-ray solution scattering as a probe of ligand-induced conformational changes in proteins," Chemistry and Biology **11**, 1431–1443 (2004).

[27] P.-C. Chen and J. S. Hub, "Interpretation of Solution X-Ray Scattering by Explicit-Solvent Molecular Dynamics," Biophysical Journal **108**, 2573–2584 (2015).